

PCCP

Accepted Manuscript



This is an *Accepted Manuscript*, which has been through the Royal Society of Chemistry peer review process and has been accepted for publication.

Accepted Manuscripts are published online shortly after acceptance, before technical editing, formatting and proof reading. Using this free service, authors can make their results available to the community, in citable form, before we publish the edited article. We will replace this *Accepted Manuscript* with the edited and formatted *Advance Article* as soon as it is available.

You can find more information about *Accepted Manuscripts* in the [Information for Authors](#).

Please note that technical editing may introduce minor changes to the text and/or graphics, which may alter content. The journal's standard [Terms & Conditions](#) and the [Ethical guidelines](#) still apply. In no event shall the Royal Society of Chemistry be held responsible for any errors or omissions in this *Accepted Manuscript* or any consequences arising from the use of any information it contains.

Insight into the Structure and the Mechanism of the Slow Proton Transfer in the GFP Double Mutant T203V/S205A

Vered Wineman-Fisher^{1,2}, Ron Simkovitch³, Shay Shomer³, Rinat Gepshtein³, Dan Huppert³, Mari Saif⁴, Karen Kallio⁴, S. James Remington⁴ and Yifat Miller^{1,2,}*

¹Department of Chemistry, Ben-Gurion University of the Negev, P.O. Box 653, Be'er Sheva 84105, Israel

²Ilse Katz Institute for Nanoscale Science and Technology, Ben-Gurion University of the Negev, Beér-Sheva 84105, Israel

³Raymond and Beverly Sackler Faculty of Exact Sciences, School of Chemistry, Tel Aviv University, Tel Aviv 69978, Israel

⁴Department of Physics and Institute of Molecular Biology, University of Oregon, Eugene, Oregon 97403-1229, USA

*Corresponding author:

Yifat Miller: ymiller@bgu.ac.il

Tel: 972-86428705; Fax: 972-86428709

Abstract

Mutations near the fluorescing chromophore of the green fluorescence protein (GFP) have direct effects on the absorption and emission spectra. Some mutants have significant band shifts and most of the mutants exhibit a loss of fluorescence intensity. In this study we continue our investigation of the factors controlling the excited state proton transfer (PT) process of GFP, in particular to study the effects of modifications to the key side chain Ser205 in wt-GFP, proposed to participate in the proton wire. To this aim we combined mutagenesis, X-ray crystallography, steady-state spectroscopy, time-resolved emission spectroscopy and all-atom explicit molecular dynamics (MD) simulations to study the double mutant T203V/S205A. Our results show that while in the previously described GFP double mutant T203V/S205V the PT process does not occur, in the T203V/S205A mutant the PT process does occur, but with 350 times slower rate than in wild-type GFP (wt-GFP). Furthermore, the kinetic isotope effect in the GFP double mutant T203V/S205A is twice smaller than in the wt-GFP and in the GFP single mutant S205V, which forms a novel PT pathway. On the other hand, the crystal structure of GFP T203V/S205A does not reveal a viable proton transfer pathway. To explain PT in GFP T203V/S205A, we argue on the basis of the MD simulations for an alternative, novel proton-wire pathway which involves the phenol group of the chromophore and water molecules infrequently entering from the bulk. This alternative pathway may explain the dramatically slowed PT of the GFP double mutant T203V/S205A compared to wt-GFP.

Keywords: Molecular Dynamics simulations, time-resolved emission spectroscopy, proton-wire pathway, steady-state spectroscopy, chromophore.

Introduction

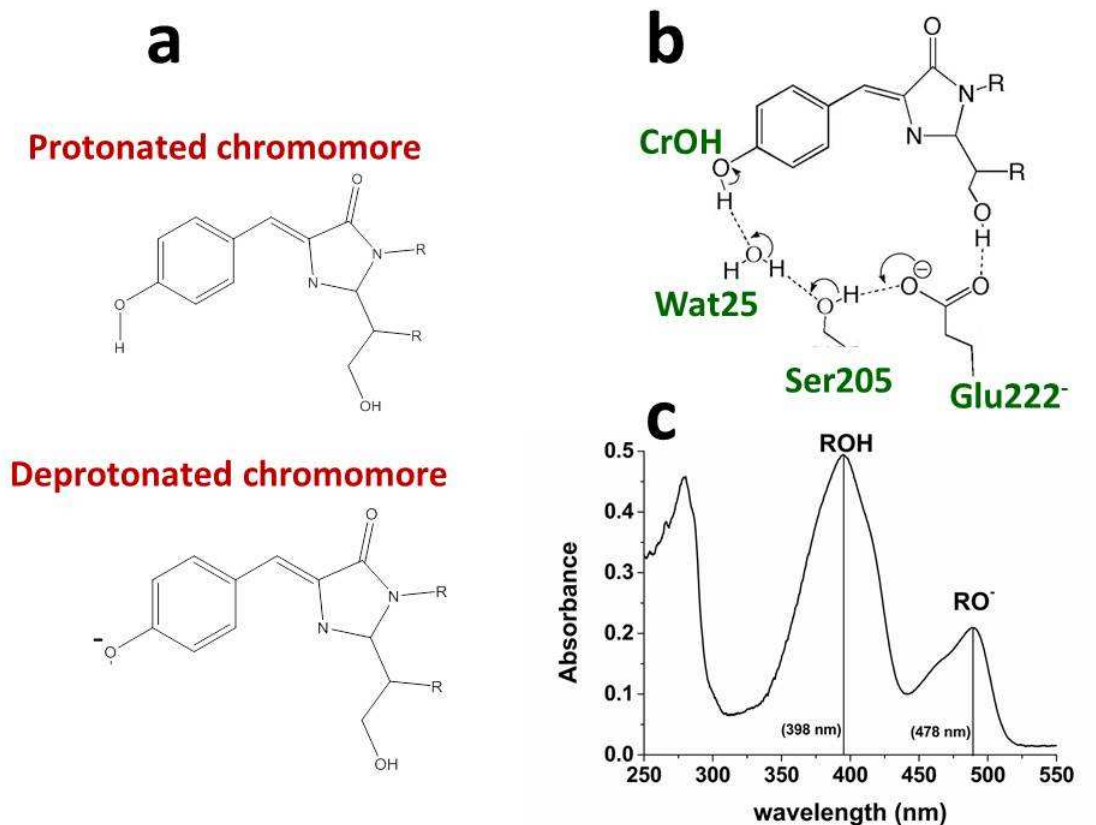
The green fluorescent protein (GFP) is a fluorescent protein isolated from coelenterates, such as the pacific jellyfish *Aequorea victoria* or from the sea pansy *Renilla reniformis*.¹ The fluorescent properties of the GFP as a biological fluorescence marker make it especially useful in living cells, gene expression and tissues.²⁻⁴ In its native system, GFP emits green light through a strong energy transfer coupling mechanism with aequorin, a calcium-induced blue photoprotein.⁵ The role of GFP is to transduce the blue chemiluminescence of the aequorin protein into green fluorescent light by energy transfer. The GFP is the prototypical example of a biological system in which excited state proton transfer (ESPT) plays a functional role in the mechanism of activity.^{6,7}

The fluorescing chromophore in GFP is 4-(p-hydroxybenzylidene) imidazolidin-5-one (HBI), which is formed by a rapid posttranslational cyclization from a short segment of three residues S65-Y66-G67.⁸ This tripeptide is part of one of the α -helices of the GFP and shields the chromophore from the environment. Therefore, the chromophore is covalently anchored and effectively separated from the aqueous solvent surrounding the protein.

The absorption spectrum (at room temperature) of wild-type GFP (wt-GFP) shows two excitation bands: a strong band A (398 nm) corresponds to the neutral protonated form ROH of the chromophore and a weak band I (478 nm) represents the anionic deprotonated form RO⁻ of the chromophore (scheme 1). In the steady state fluorescence spectrum the excitation of anionic form of wt-GFP leads to a strong fluorescence emission band 510 nm and a weak band at 460 nm. Previously Remington and coworkers⁹ proposed the ESPT emission process as seen in scheme 1.

The GFP can be re-engineered by mutagenesis to ameliorate undesirable properties, such as low brightness. These engineered GFPs can shift both the excitation and emission wavelengths, creating different colors and new applications. Random and site-direct mutagenesis produced potentially useful mutants with single and multiple amino acid substitutions that exhibit excitation and emission spectra different from those of wt-GFP. For example, mutants that shift the absorption and emission peaks which allow multiple labeling are required for protein colocalization experiments. Spectrally, shifted GFP mutants may also be useful for studying protein-protein interactions by fluorescence

resonance energy transfer (FRET) methods.¹⁰ A blue shifted double mutant Y66H/Y145F has proven to be useful in two channel fluorescence experiments.¹¹ Further blue-shifted appears in the triple mutant F64/Y66H/V68I, which has exhibited from FRET.¹² Finally, a red-shifted mutant T203Y/S65G/V68L/S72A has been reported with limited spectral separation from other GFPs.¹³

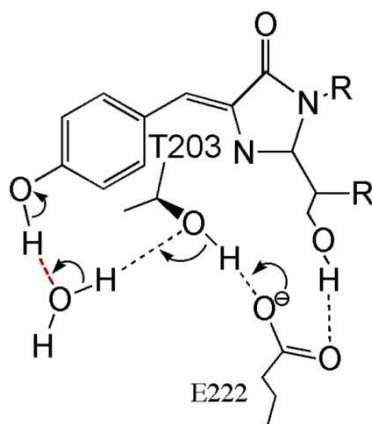


Scheme 1: (a) Protonated and deprotonated forms of the chromophore (b) Schematic diagram of the proton wire in wild-type GFP (c) Spectra of protonated and deprotonated forms of the chromophore for the wt-GFP.

In the last decade photophysical studies of various GFP mutants have shown that the five residues S65, H148, T203, S205 and E222 which are located in the vicinity of the chromophore are crucial in the protolytic acid-base equilibrium both in the ground state and the ESPT rate.¹⁴ Interestingly, Jung et al¹⁵ investigated the photophysics of the GFP by performing mutations in S65, T203 and E222. The GFP E222Q mutant showed that the ground state equilibrium between the protonated and the deprotonated forms of the chromophore is dramatically changed and the deprotonated form is more stable than the

protonated form. Using picosecond time-resolved mid-infrared absorption van Thor et al.¹⁶ found that the ESPT emission process in GFP E222D mutant is slower than in wt-GFP and the kinetic isotopic effect (KIE) is larger than in wt-GFP. At the same time, Stoner-Ma et al. provided strong direct evidence that E222 is the proton acceptor, in that protonation of E222 occurs with the same kinetics as deprotonation of the chromophore.¹⁷ These findings indicate that E222 is crucial in the proton transfer (PT) process. However, a number of questions remain concerning the role of other side chains in the process, such as S205. For example, is proton transfer concerted or stepwise, and if stepwise, what is the nature of the intermediate(s)?

In our previous studies we investigated the structure and the ESPT emission process of GFP S205V mutant using steady state emission spectroscopy, time-resolved emission techniques, x-ray crystallography and molecular dynamics (MD) simulations.^{18,19} These combined techniques illustrated that the S205V mutation blocks the proton wire as shown in the wt-GFP. However a structural rearrangement led an alternative proton wire that showed 30 times slower PT than that of wt-GFP (scheme 2). Furthermore, the KIE of the PT rate for the GFP S205V mutant is around 5, similarly to the KIE of the wt-GFP. We then showed that in the double mutant GFP S205V/T203V the alternative proton transfer pathway is eliminated, resulting in a novel blue fluorescent protein.



Scheme 2: A schematic diagram of the proton wire in S205V mutant of GFP observed from X-ray crystallography (Ref. 18).

In this study, we combined mutagenesis, x-ray crystallography, steady state and time-resolved emission spectroscopy and MD simulations in aim to investigate whether the PT

process occurs in the GFP double mutant T203V/S205A and if it occurs, by what proton transfer pathway. Our results showed that while in the GFP double mutant T203V/S205V the PT process does not occur, the GFP double mutant T203V/S205A does undergo a PT process, but with ~30 times slower rate than GFP S205V and with dramatically (~350 times) slower rate than wt-GFP. The KIE in the GFP double mutant T203V/S205A is twice smaller than the wt-GFP. We propose in this study a novel pathway in which the proton wire involves the H atom of the phenol group of the chromophore and water molecules from the bulk. This proposed pathway may explain the dramatically slow PT in the T203V/S205A compared to the wt-GFP.

Materials and Methods

Mutagenesis, protein expression, and crystallization

Site directed mutagenesis was used to prepare the mutant GFP T203V/S205A. We started with the construct for the double mutant GFP T203V/S205V described previously¹⁸ and used the QuickChange™ method with the following primers to prepare modified cDNA (where the upper case letters indicate the base changes from the original, required to introduce the S205V→A amino acid sequence change).

203V/205A_1:

5' ccattacctgtccgtacaagCGgccctttcgaaagatccc 3'

203V/205A_2:

5' gggatctttcgaaagggcCGcttgtacggacaggtaatgg 3'

The cDNA produced was sequenced in its entirety to verify that the desired mutations, and no other, had been introduced. Protein expression and purification were performed as described by Shu et al.¹⁸ Briefly, protein was expressed in Escherichia coli strain JM109 (DE3), by use of the PRSETB His-tagged expression system. Protein was purified by Ni²⁺-affinity chromatography over Ni-NTA agarose (Qiagen), and then buffer exchanged with PD-10 Sephadex columns (Amersham Pharmacia) into 50 mM HEPES (pH 7.9). Surprisingly, the GFP T203V/S205A mutant protein was visibly blue/green fluorescent, suggesting that although the ESPT pathway should be disrupted by the mutation, proton transfer nevertheless takes place. Crystals were produced with the hanging drop vapor

diffusion method using 1 μL protein (26 mg/ml in 0.1 M imidazole, pH 7.8) mixed with 1 μL well solution. Crystallization screens varied from 22% to 32% (w:v) polyethylene glycol monomethyl ether (PEG) 2000 and 0.05M to 0.2M KBr at room temperature, for a range of pH values near neutrality. Crystals for cryogenic data collection were prepared under the following conditions: 32% PEG 2000 and 0.2M KBr, pH 7.4 at room temperature, dipped in paratone, and flash frozen in a stream of dry nitrogen gas at 100 K.

Data collection and structure solution

Diffraction data were collected on an in-house rotating anode X-ray source (Rigaku RU-3H, wavelength 1.54 Å) and collected using an R-Axis IV image plate detector, from a single flash frozen (100 K) crystal to 2.22 Å resolution (Table 1). The mosaicity of the crystal was rather high at 1.3°, consequently the diffraction data are not of the best quality, consistent with an Rmerge of over 9%. The space group was determined from the diffraction pattern to be tetragonal, P422 or related. The molecular locations were discovered and the absolute configuration was determined to be P41 21 2 by molecular replacement using the program EPMR.²⁰ The starting model for molecular replacement and for protein structure refinement was that of the single mutant GFP S205V described by Shu et al.¹⁸ (RCSB Protein Data Bank ID 2QLE, chain A).

Table 1. Summary of crystallographic statistics

GFP S205A/T203V	
Data collection and crystal	
Total reflections	827,879
Unique reflections	27,559
Space Group and cell (a, b, c) (Å)	P 41 21 2 (86.6,86.6,119.2)
Resolution (Å)	33-2.22

Highest resolution shell (Å)	2.26-2.22
Completeness ^a (%)	99.9 (99.5)
Average I/σ^a	31.3 (3.2)
Mosaicity (°) and Wilson B (Å ²)	1.3, 43
$R_{\text{merge}}^{\text{a,b}}$	0.094 (0.780)
Refinement	
Refinement resolution limits (Å)	15-2.30 (2.39-2.33)
Reflections ($I > 2 \sigma(I)$)	14381 (134)
Number of protein chains ^c	2
No. of protein atoms ^c	3521
No. of solvent atoms ^c	157 H ₂ O + 1 Cl
Crystallographic R -factor ^d	0.185 (0.28)
R -free ^e	0.303 (0.37)
Combined	0.190
Average B -factors (Å ²)	56
Protein atoms	56
Solvent	58
rmsd bond lengths (Å)	0.01
rmsd bond angles (degrees)	1.6
B -factor correlations (Å ²)	4.6

^a Values in parentheses indicate statistics for the highest resolution data shell

^b $R_{\text{merge}} = \Sigma(|I - \bar{I}|) / \Sigma I$ where I is the observed intensity, and \bar{I} is the average of intensities

^cPer asymmetric unit.

^d $R\text{-factor} = \Sigma||F_o| - |F_c|| / \Sigma|F_o|$, where F_o and F_c are the observed and calculated structure amplitudes.

^e $R\text{-free}$ calculated for 5% of unique reflections (1193)

According to the crystal unit cell parameters and packing arguments, there should be two independent copies of GFP T203V/S205A in the asymmetric unit of the crystal, and this was confirmed with EPMP. Thus the crystal affords two independent views of the molecular structure. Refinement proceeded with the CCP4 suite of crystallographic programs²¹ using REFMAC5^{22,23} while manual rebuilding was performed with COOT.²⁴ Restraints on noncrystallographic symmetry were not applied, but the final overall rms deviation between the alpha-carbon atoms in the two copies of the molecule in the asymmetric unit is 0.29 Å, which is comparable to the level of error in the structure determination.

The final model statistics for GFP T203V/S205A are presented in Table 1. The final crystallographic working R-factor is 0.18 for data between 15 and 2.3 Å resolution and the model has excellent geometry. We attribute the unexpectedly high Rfree of about 0.30 to the very high mosaicity and poor data quality of the crystals. Regardless, the electron density map was clear and both subunits in the asymmetric unit showed the same density profile, consistent with the introduced mutation. The atomic model for GFP T203V/S205A has been deposited in the RCSB Protein Data Bank and is accessible under PDB ID 4OGS.

Steady state spectroscopy

Samples of the GFP double mutant T203V/S205A at a concentration of about 2 mg/ml, including 0.3 M NaCl, were stored under refrigeration. Samples were prepared by

dilution of the stock solution, with either H₂O buffer solution or D₂O, by a factor of about 5-10. The absorbance at 397 nm was typically between 0.1-0.3 OD. Steady-state fluorescence was measured using a FluoroMax-3 Spectrofluorimeter (Jobin Ivon). 99.8% isotopically pure D₂O was purchased from Aldrich. Deionized water (resistivity > 10 MΩ/cm) was used.

Time-resolved emission spectroscopy

For excitation of GFP samples we used a cavity-dumped mode-locked Ti: sapphire femtosecond laser (Mira Coherent), which provides short, 150 fs, pulses of variable repetition rate. We used the SHG frequency, over the spectral range of 380 – 440 nm. Time-resolved fluorescence was acquired using the time-correlated single-photon counting (TCSPC) technique, the method of choice when sensitivity, large dynamic range and low intensity illumination are important criteria in fluorescence decay measurements. The TCSPC detection system is based on a Hamamatsu 3809U, photomultiplier and Edinburgh instruments TCC 900 computer module for TCSPC. The overall instrumental response was about 40 ps (fwhm). Measurements were taken at 10 nm spectral width. The large dynamic range of the TCSPC system (more than 4 orders of magnitude) enabled us to accurately determine the non-exponential photoluminescence decay profiles of the wt-GFP and the mutant's fluorescence.

The excitation pulse energy was reduced by neutral density filters to about 10 pJ. We checked the sample's absorption prior to and after time-resolved measurements. We could not find noticeable changes in the absorption spectra due to sample irradiation. The time-resolved emission decay curves of the T203V/S205A samples were the same after repeated experiments. We thus conclude that, under our irradiation condition, no sample deterioration could be detected.

Molecular dynamics (MD) simulations protocol

Molecular dynamics (MD) simulations were performed starting from the crystallographic structure of the GFP double mutants T203V/S205A. We performed a mutation for the S205 to the latter mutant to form the double mutant T203V/S205V. MD simulations of the solvated structures were performed in the NPT ensemble using the NAMD²⁵ with the

CHARMM27 force field.²⁶ The GFP chromophore lacks a parameter set in the CHARMM27 force-field; therefore we made a parameter set for the chromophore as previously done by Vendrell et al.²⁷ and Simkovitch et al.¹⁹ The structures were energy minimized and explicitly solvated in a TIP3P water box^{28,29} with a minimum distance of 15 Å from each edge of the box. Each water molecule within 2.5 Å of the protein was removed. Counter ions (Na⁺ and/or Cl⁻) were added at random locations to neutralize the protein's charge. The Langevin piston method^{25,30,31} with a decay period of 100 fs and a damping time of 50 fs was used to maintain a constant pressure of 1 atm. The temperature 310 K was controlled by a Langevin thermostat with a damping coefficient of 10 ps.²⁵ The short-range van der Waals (VDW) interactions were calculated using the switching function, with a twin range cutoff of 10.0 and 12.0 Å.^{32,33} Long-range electrostatic interactions were calculated using the particle mesh Ewald method with a cutoff of 12.0 Å.^{32,33} The equations of motion were integrated using the leapfrog integrator with a step of 1 fs. The counter ions and water molecules were allowed to move. The minimized solvated systems were energy minimized for 5000 additional conjugate gradient steps and 20,000 heating steps at 250 K, with all atoms allowed to move. Then, the system was heated from 250 to 310 K for 300 ps and equilibrated at 310 K for 300 ps. In addition to the 300 ps of equilibration using the CHARMM program, we also performed equilibration using the NAMD program for 1 ns. The structures were converged and then, the converged structures were simulated for 60 ns. RMSD and RMSF calculations of the two double mutant variants illustrated convergence of the structure (Figures S1 and S2). The simulations ran for 60 ns and the structures were saved every 10ps for analysis. The long-timescale of the simulations and the short-timescales of saving coordinates are reasonable to perform analysis.

Results and Discussion

Crystal Structure of GFP T203V/S205A

As expected, the crystal structure of GFP T203V/S205A is extremely similar to that previously described for GFP S205V. Overall, the structures superpose, atom by atom, to about 0.2 Å rms, (which is at the level of the coordinate error of both investigations) however some structural changes near the site of the mutation were clearly evident in the

electron density map and common to both protomers in the asymmetric unit. Figure 1 shows an overlay of the final atomic models of the two structures in the immediate vicinity of the mutation. In Figure 1 one can see that, compared to S205V, the main chain and side chain of S205A (green backbone) moves in toward the chromophore in response to the reduction in size of the 205 side chain. Furthermore, E222, which is the ultimate ESPT proton acceptor in wt-GFP, moves away from its position in S205V, together with the Ser side chain of the chromophore but maintaining the hydrogen bond between them. E222 evidently moves to lengthen the distance between its side chain and that of the introduced V203, as a hydrogen bond cannot form between the Glu and Val side chains, as found between the carboxylate of E222 and the hydroxyl of T203 (blue backbone). There is a single water molecule (labeled H₂O in Figure 1) trapped in the chromophore cavity, in hydrogen bonding distance to the chromophore phenolic hydroxyl group. In the *time averaged, flash frozen* crystal structure, no other water molecules are observed close to the chromophore hydroxyl group, and no proton transfer pathway is evident between the hydroxyl group of the chromophore and E222.

To assess the possibility that there may be solvent molecules that are in the chromophore cavity but poorly localized and thus not evident in the electron density map, we used the program MSROLL by M. Connolly³⁴ to determine the locations of internal cavities within the protein. The probe radius was 1.4 Å, which is slightly smaller than the standard value (1.5 Å) used as the radius of a water molecule probe. The same calculation was repeated for the mutant GFP S205V. In both cases, no cavities capable of accommodating a water molecule were found near the chromophore. We conclude from this simple analysis that both protein structures are well-packed, and that no water molecules capable of proton transfer were overlooked in the model building process.

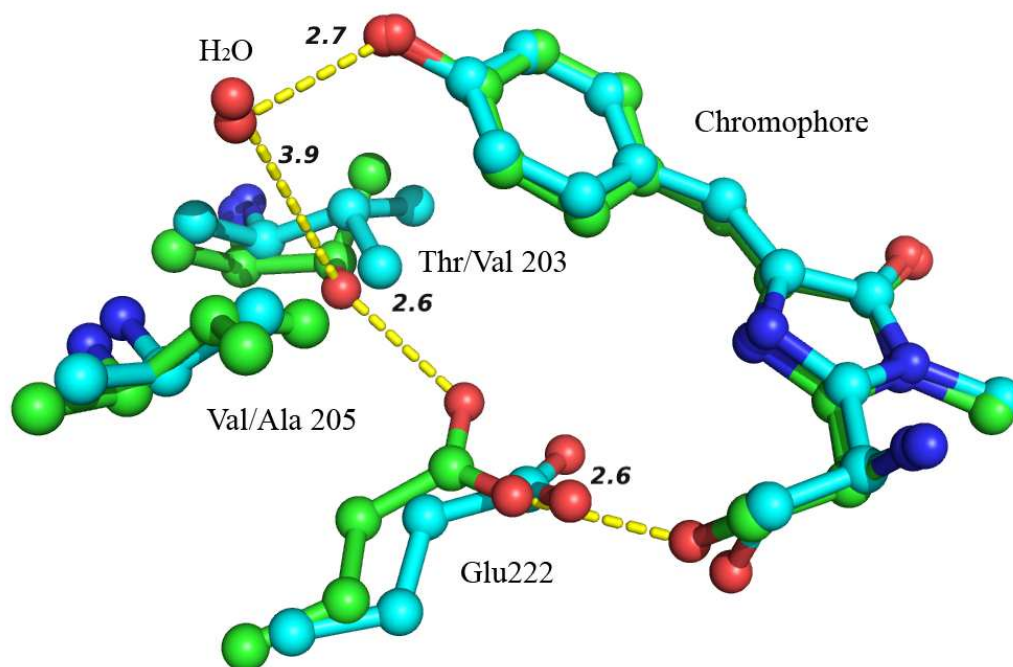


Figure 1: Overlay of selected portions of the atomic models for GFPs S205V (green backbone, which contains an inefficient, non-native proton transfer pathway) and T203V/S205A (blue backbone, which does not contain a readily discernable proton transfer pathway). Note: the crystal structure of the double mutant T203V/S205V has not been determined and is unavailable for comparison. Selected hydrogen bonds forming the inefficient proton transfer pathway in GFP T203/S205V are shown as dashed lines and have the indicated lengths in Å. Atoms are represented as spheres with oxygen red and nitrogen dark blue. The two isolated red spheres correspond to structurally equivalent water molecules, trapped adjacent to the chromophore hydroxyl group in both crystal structures.

The slow proton transfer rate in the GFP double mutant T203V/S205A depends on the kinetic isotope effect (KIE)

In the ground state, the wt-GFP chromophore is mostly in the protonated form whereas the glutamic acid E222 is ionized in the deprotonated form. In the double mutant T203/S205A the chromophore is almost exclusively in the protonated ROH form. The absorption spectrum of GFP double mutant T203V/S205A exhibits a major band A at ~ 388 nm, which is attributed to the protonated ROH form of the chromophore and a minor band I at ~ 500 nm, which is attributed to the deprotonated RO^- form (Figure 2). The ratio between the absorption intensities of the bands A:I in the mutant is 30:1, whereas in the wt-GFP it is 4:1.

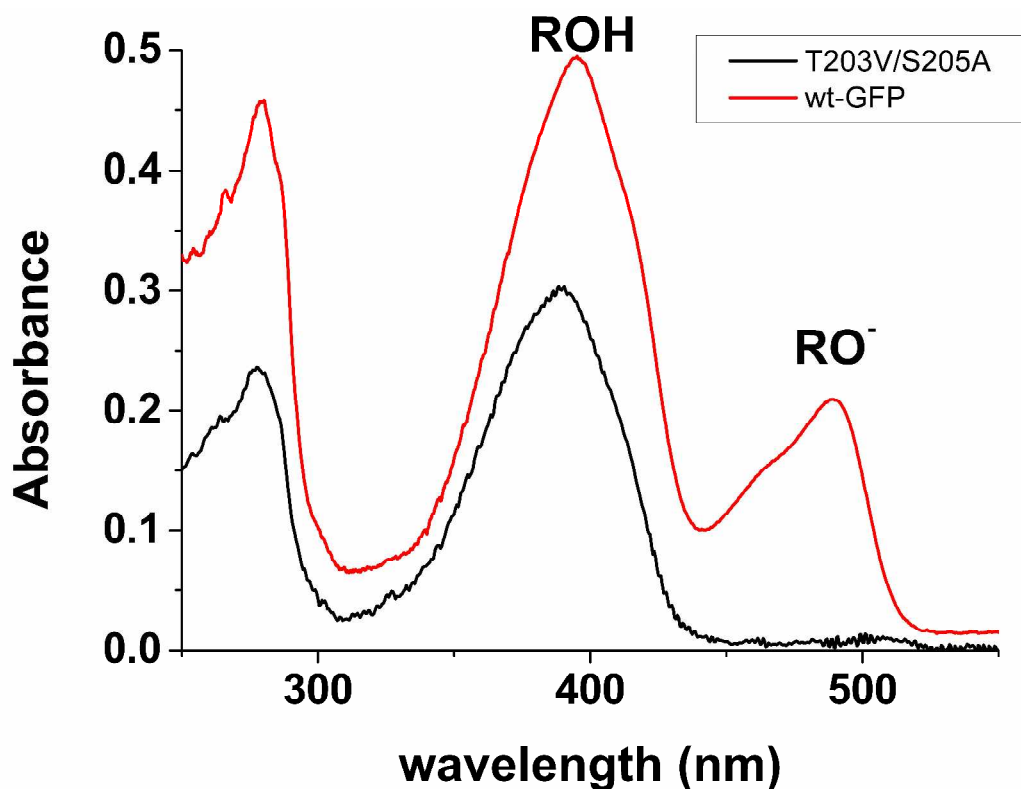


Figure 2: Steady-state absorption spectrum of GFP double mutant T203V/S205A in pH=7 (black) and wt-GFP (red), please note that the measurements were not made at the same concentration.

Excitation at 400 nm – near the A band peak, leads to a steady-state (time-integrated) emission spectrum that consists of two emission bands. The protonated emission band is broad with an emission band peak at about 460 nm and the deprotonated RO^- emission band which is more narrow with an emission at 517 nm, slightly red shifted with respect to the peak position of the wt-GFP (512 nm). Taking into account the large overlap between the emission bands, the ratio between the peak intensities of bands A:I is 0.6:1. (Figure 3a). Upon deuteration this ratio increases to 1:0.8 (Figure 3a). The difference in the peak intensity ratio between bands A and I in H_2O and D_2O is attributed to the kinetic isotope on the PT rate. This result indicates that the PT rate is strongly dependent on the KIE. Furthermore, the nonradiative rate of the ROH form which shows similar value rate in H_2O and D_2O does not demonstrate the largest value rate.

Excitation at 475 nm – near the I absorption band, which is attributed to the deprotonated form of the chromophore RO^- , exhibits a typical emission band shape that exists in wt-GFP and also in most of the GFP mutants. This band shape consists of two distinguished sub-vibration bands: a strong band at 517 nm and a strongly weaker band at 550 nm (Figure 3b). The ratio between the intensities of these two sub-bands is $\sim 4:1$. Upon deuteration, similar sub band intensities had been observed in the steady state emission spectrum (Figure 3b). However, the deuteration shows a slight red shift by 2 nm of band I. This result has been found also for the wt-GFP and other single mutants.

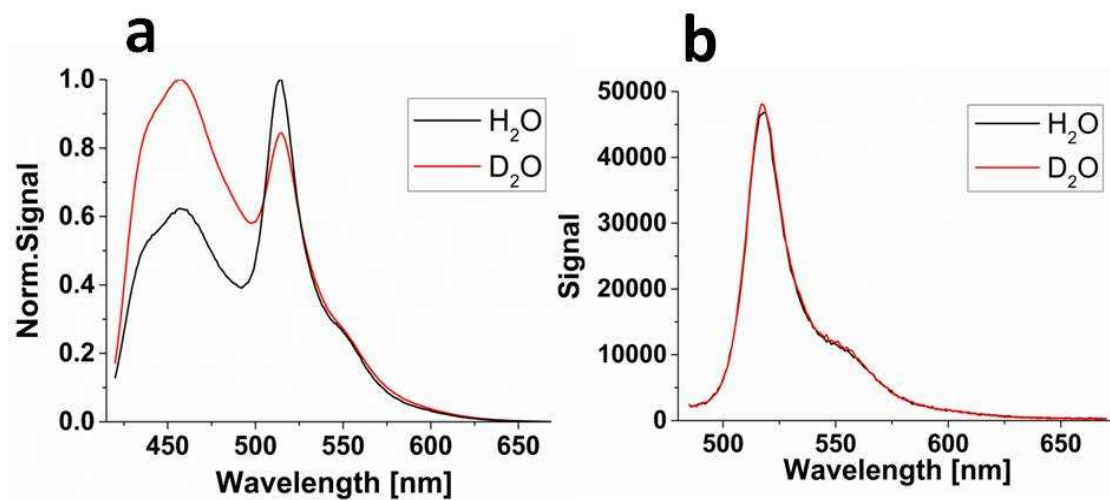


Figure 3: Steady state emission spectra of GFP double mutant T203V/S205A in H₂O and D₂O in pH=7, excited at 400 nm, near the absorption peak of band A (a) and at 475 nm, near the absorption peak of band I (b).

We further performed a fitting of the bands of the steady state emission spectra assigning a lognormal band shape function³² for each vibronic sub level (or sub bands). We fitted the ROH band with three sub bands whereas the RO⁻ emission band by only two sub bands. Figure 4 illustrates the experimental steady state spectra and the fitted vibronic sub levels for the GFP double mutant T203V/S205A.

The ratios between the intensities of the A emission sublevels are 0.86:1:0.28. This intensity ratio of the sub bands arises from a large Huang Rhys factor $S_0 > 1$.³⁵ When $S_0 > 1$, the intensity of the second vibronic level band is stronger than that of the first. In a one dimensional potential surface picture of the ground and excited electronic states, a large shift of the minimum position of the excited state parabola from the ground state minimum position (with respect to the curvature of the parabolas) lead to a large Huang Rhys factor.³⁵ Such large S factor enables in the excited state a larger interaction of a certain mode of the ROH with its surroundings. One such plausible mode is a one that is strongly coupled to the large acidity of the chromophore in the excited state.

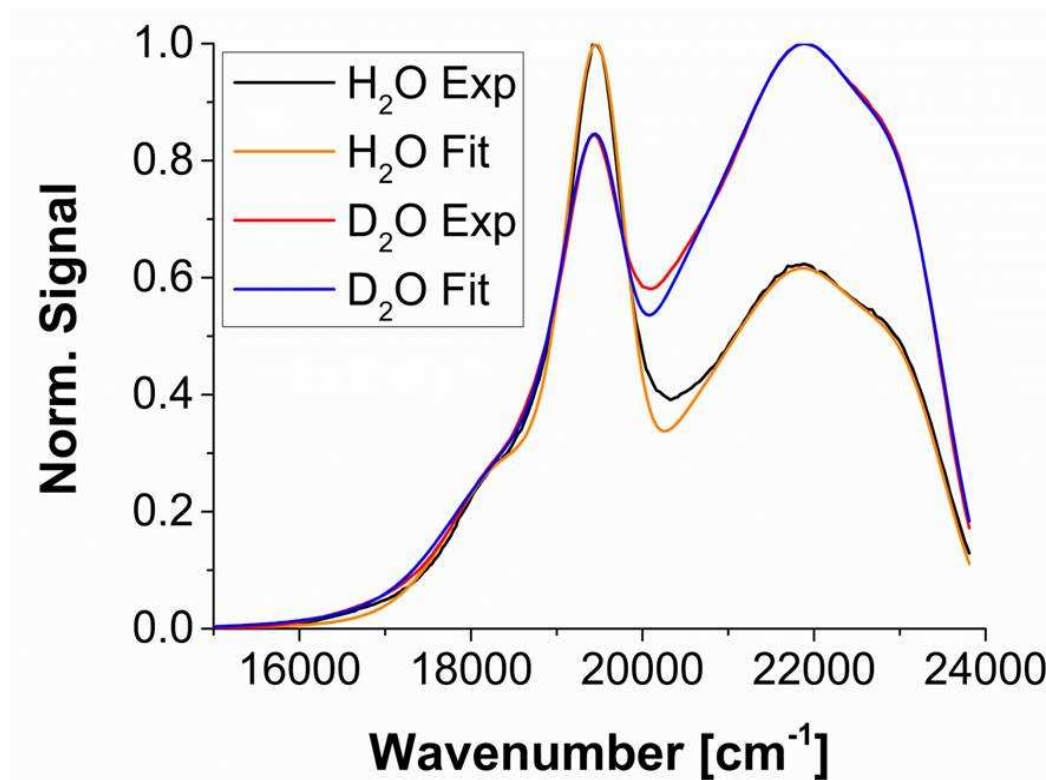


Figure 4: Steady-state emission spectra and fitting emission spectra of GFP double mutant T203V/S205A in H₂O and D₂O.

Upon deuteration the PT KIE is 2.75 (Figure 4). The relatively large KIE and supports the conclusion that PT occurs in the double mutant. Previously, it has been shown that the KIE on PT of the wt-GFP and other single mutants such as S205V is ~5 (Figure S3).

Spectral fitting procedure for bands A and I in the steady state spectra

Each emission band is modeled by two vibrational bands. The shape of the absorption bands of large dye molecules in polar solvents is fitted by a log-normal line-shape function with four adjustable parameters.³⁶ The emission band intensity at frequency ν is given by

$$I(\nu) = h \begin{cases} \exp\left[-\ln(2)\left\{\frac{\ln(1+\alpha)}{\gamma}\right\}^2\right] & \alpha > -1 \\ 0 & \alpha \leq -1 \end{cases} \quad (1)$$

$$\alpha \equiv 2\gamma(\nu - \nu_p)/\Delta \quad (2)$$

Where h is the peak height (amplitude), ν_p is the peak position, γ is the asymmetry parameter and Δ is the band width. These four adjustable parameters describe an asymmetric line shape. When $\gamma=0$ the line-shape is a Gaussian. Table 2 provides the fitting parameters of the log-normal fit function of the steady state spectra.

Table 2. Fitting parameters of the lognormal fit of the steady-state emission of T203V/S205A^a

		h_1	ν_{p_1} (cm^{-1})	$\Delta\nu_{p_1}$ (cm^{-1})	h_2	ν_{p_2} (cm^{-1})	$\Delta\nu_{p_2}$ (cm^{-1})	h_3	ν_{p_3} (cm^{-1})	$\Delta\nu_{p_3}$ (cm^{-1})
H ₂ O	ROH band	1.00	22750	1800	0.73	21440	1800	0.21	20200	1800
	RO ⁻ band	1.00	19450	1300	0.25	18300	1300	-	-	-
D ₂ O	ROH band	1.00	22750	1800	0.71	21440	1800	0.25	20200	1800
	RO ⁻ band	1.00	19400	1300	0.23	18220	1300	-	-	-

^a The asymmetry parameter:

$$\gamma_{\text{ROH}} = 0.3$$

$$\gamma_{\text{RO}^-} = -0.15$$

Time-resolved emission

The time-resolved emission was acquired by excitation of the mutants with short laser pulses and using the time-correlating single photon counting (TCSPC) technique. Figures 5a and 5b show the time-resolved emission decay of the band A of T203V/S205A mutant, which is assigned to the protonated form of the chromophore and measured at 450 nm, and the emission decay of band I, which is assigned to the deprotonated RO⁻ form of the chromophore and measured at 515 nm. One can see that A band decay is a non-exponential, in which its average emission life-time decay is ~ 0.8 ns, while the I band signal shows an increased component followed by an exponential decay (Figure 5b) and exhibits an average emission life-time decay of 3.3 ns. Previously, it has been shown

that the emission life-time decay of band A in the wt-GFP is 10 ps, which is 100 times faster than that of the GFP double mutant T203V/S205A.

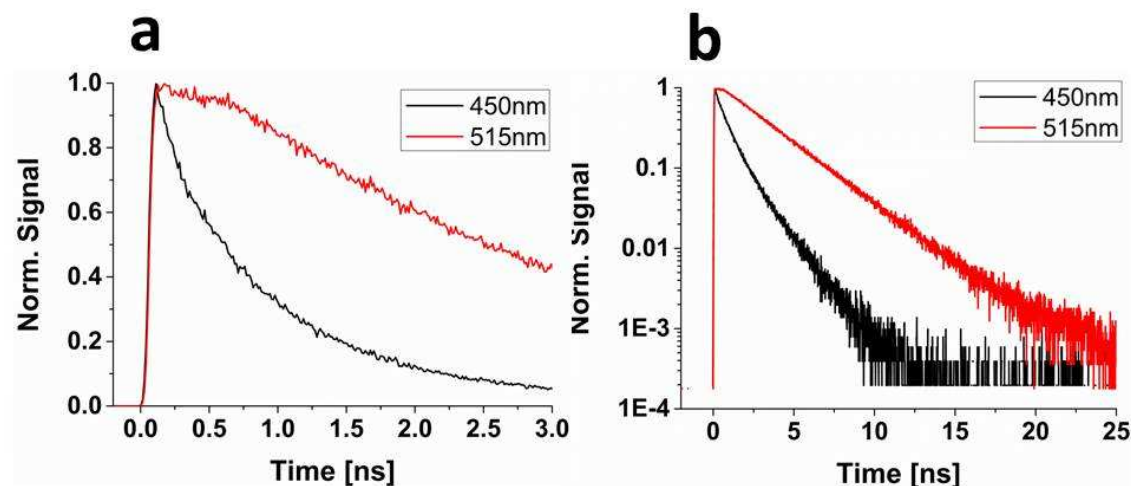


Figure 5: Time-resolved emission spectra of GFP double mutant T203V/S205A in H₂O, on a linear scale (a) and semilogarithmic scale (b).

Upon deuteration at short timescales up to about $t > 0.2$ ns, the emission decays measured at 450 nm and 517 nm, the peak positions of the A and I bands, are similar. However at longer times $t > 0.2$ ns the non-exponential average decay time of band A is ~ 1 ns, whereas the non-exponential average decay time of band I is at longer ~ 3 ns (Figures 6a and 6b). Upon the deuteration solvent the PT process is slower and the decay time is longer (~ 1 ns) than in the water solvent (~ 0.8 ns), as seen in Figure 6c and 6d, thus the non-radiative and the radiative rate efficiency are comparable with the PT rate in water ($k_{PT} \sim k_{nr}, k_r$) but in D₂O $k_{PT} < k_{nr}$. Therefore, the competition between the radiative and the non-radiative processes with the PT process in D₂O prevents the appearance of the emission decay of the excited deprotonated form at 515 nm. Consequently, the emission decay at 515 nm in D₂O is strongly influenced by the overlap between bands A and I. Upon deuteration at short timescales band A is more dominant, and therefore the emission decays at 450 nm and 515 nm in D₂O samples are similar. At longer timescales band I is more dominant and the emission decay of band A is ~ 1 ns and faster than the emission decay of band I, which is ~ 3 ns.

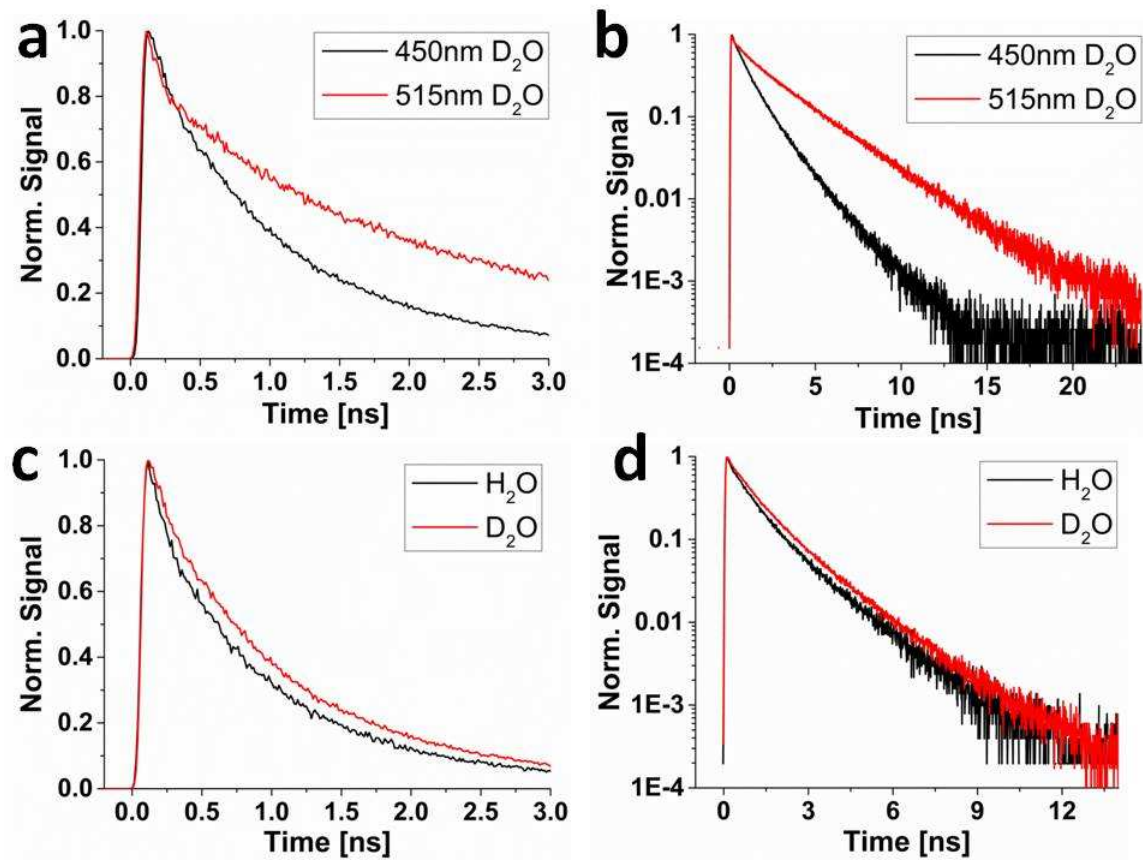


Figure 6: Time-resolved emission spectra of GFP double mutant T203V/S205A measured in D_2O in linear scale (a) and semilogarithmic scale (b). Time-resolved emission spectra of GFP double mutant T203V/S205A measured at 450 nm (near band A) in D_2O and H_2O in linear scale (c) and semilogarithmic scale (d).

Previously, we have suggested that the PT process does not occur in the GFP double mutant T203V/S205V.¹⁸ Figures 7a and 7b show the time-resolved emission of T203V/S205V in water, excited at 390 nm and the emission is measured at four wavelengths in the spectral region (450-550 nm) that consists of the spectra of both the A (ROH) and I (RO⁻) emission bands. The signals are similar and independent of the monitored wavelength. The steady-state emission spectrum shows exclusively the spectrum of the A band with no trace of the I band. Based on the steady-state and time-resolved emission experimental results, we conclude that ESPT does not occur in T203V/S205V double mutant. In the time-resolved emission signal of T203V/S205A

mutant the protonated form (band A) measured at 450 nm one can see that the emission decays for both in D₂O and water are similar (Figures 6c and 6d). In the deuterated solvent the average emission life-time is slightly longer, with a decay time $\tau_F = 1$ ns, than in the water solvent ($\tau_F = 0.8$ ns). The time-resolved emission measured at 515 nm consists of a contribution from both A and I bands. Figure 7a shows the time-resolved emission measured at 515 nm of the mutant in both D₂O and water solvents. One can see that the emission decay of T203V/S205A mutant in water is longer than the emission decay in the deuterated solvent. The explanation for this peculiar result is because of the relatively large amplitude of the band A emission at $\lambda=515$ nm in the D₂O compared to the amplitude of this band in H₂O. In D₂O $k_{PT} < k_r$, thus Φ_{PT} is small and most of the signal originates from the A band (also at 515 nm - the I band maximum) and not from the I band, as expected for a large k_{PT} value (i.e. $k_{PT} > k_r$). The signal of the A band is shown in Figure 6a.

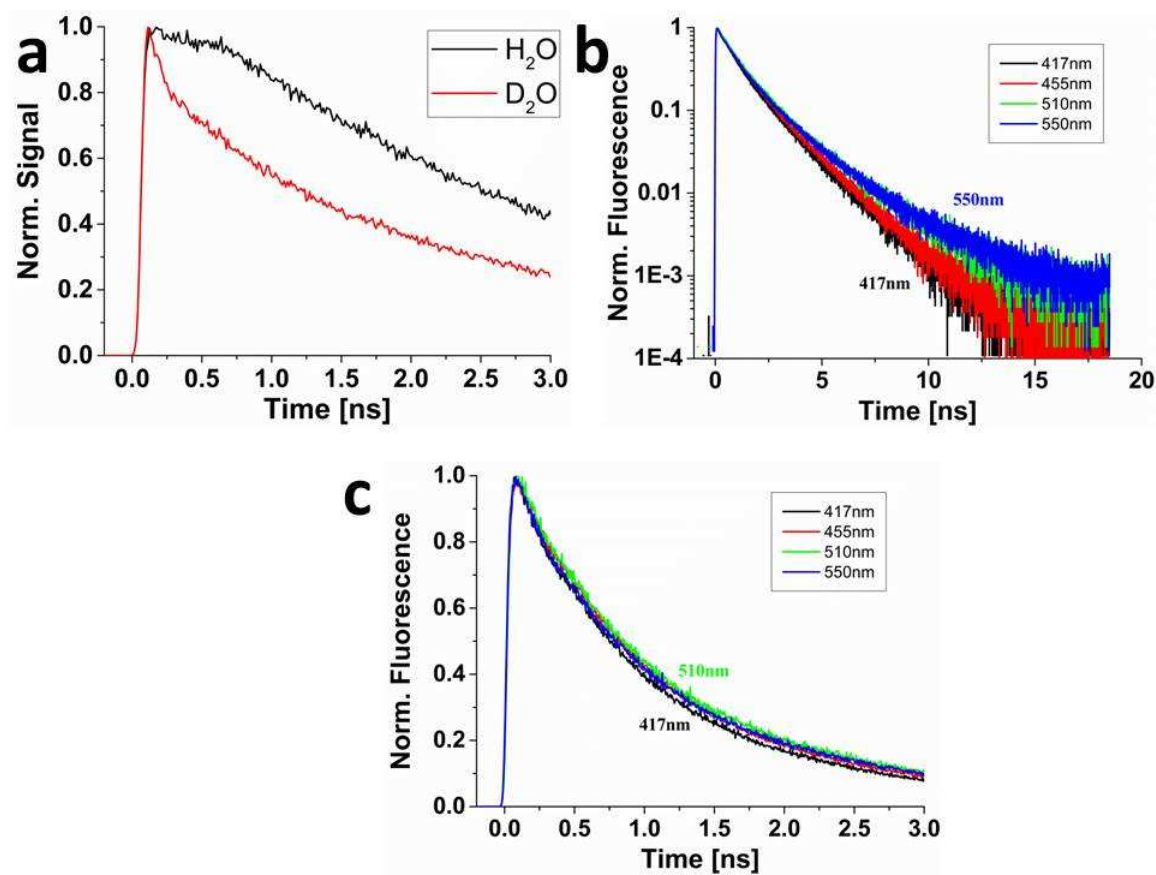


Figure 7: Time-resolved emission spectra of (a) GFP double mutant T2032V/S205A measured in D₂O and H₂O at 515 nm (near band I) in linear scale. (b) GFP double mutant T203V/S205V in H₂O Ex at 390nm ; Wavelength dependence semilogarithmic scale. (c) GFP double mutant T203V/S205V in H₂O Ex at 390nm ; Wavelength dependence linear scale.

The proton transfer process in the wt-GFP is dramatically faster than in the GFP double mutant T203V/S205A

It is of a great interest to compare the time-resolved emission TCSPC signals of the wt-GFP to that of the GFP double mutant T203V/S205A. Figures 8a and 8b illustrate the differences between these two signals for the protonated form of the chromophore (band A) and the deprotonated form of the chromophore (band I). While for the deprotonated form both wt-GFP and the mutant show similar life-time decays of ~ 3 ns, the decay of the protonated form of the wt-GFP is 10 ps. This short time (shorter than the instrument response (IRF) of the TCSPC system with an IRF of 40 ps) is dramatically faster by 100 times than the decay of the double mutant, that its value is ~ 1 ns.

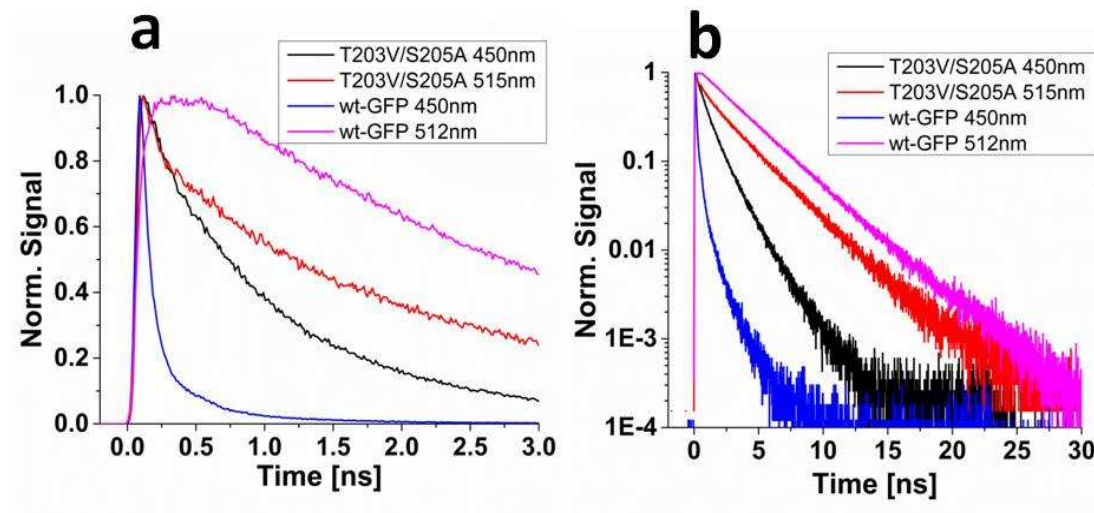


Figure 8: Time-resolved emission spectra of wt-GFP and GFP double mutant T203V/S205A in D_2O in linear scale (a) and in semilogarithmic scale (b).

The decay of the deprotonated form of the GFP double mutant T203V/S205A at short time scales $t < 0.4$ ns, is shorter than the decay of the RO^- of the wt-GFP. We estimated the PT rate of the S205A/T203V double mutant by the following procedure. The ratio between the fluorescence quantum yields of the RO^- emission of the mutant when excited from the ROH and RO^- is $\Phi_{exROH}^{RO^-} / \Phi^{RO^-} = 20$. The ratio between the absorption bands of the protonated and the deprotonated forms of the mutant is $A_{ROH} / A_{RO^-} = 20$. Therefore according to equation 8, $k_{PT} \sim k_r$, i.e, the PT rate constant is similar to the radiative rate constant. Since the radiative rate constant for the mutant is $k_r = 3 \times 10^8 \text{ sec}^{-1}$, the PT rate constant is also $k_{PT} \sim 3 \times 10^8 \text{ sec}^{-1}$. The PT rate of the wt-GFP is $k_{PT} \sim 1.2 \times 10^{11} \text{ sec}^{-1}$. Therefore, the PT rate of the mutant is slower by a factor of 400 than the PT rate of the wt-GFP. Finally, the non-radiative rate constant of the protonated form of the chromophore is twice larger than the radiative rate constant and the PT rate constant, and the value of k_{nr} is $\sim 6 \times 10^8 \text{ sec}^{-1}$.

Estimation of the proton transfer rate

Previously, using steady state emission spectra we have shown that the crystal structure of the GFP double mutant T203V/S205V does not support ESPT reactivity.¹⁸ The

emission spectrum of this mutant is blue while in the wt-GFP the emission spectrum shows a strong green fluorescence which originates from the fast ESPT process. Similarly to the crystal structure of the GFP double mutant T203V/S205V the crystal structure of the GFP double mutant T203V/S205A does not support PT. The combined mutations T203V and S205V or T203V and S205A within the GFP block the proton wire that connects the chromophore with E222 as is connected in wt-GFP (as seen in scheme 1). These combined mutations also block the alternative proton wire that had been found for the single mutations of GFP S205V and GFP S205A (as seen in scheme 2), these showed a slower PT rate in comparison to the wt-GFP. Interestingly, while the steady state emission spectrum of the GFP double mutant T203V/S205V does not show an ESPT process, the steady state emission spectrum of the GFP double mutant T203V/S205A does show an ESPT process.

The PT rate can be easily determined from the time-resolved emission signal of band A measured at 450nm and indicative of the excited ROH form of the chromophore, and for the I band, that is measured at 510 nm and assigned to the RO⁻ form of the chromophore. The steady-state emission band ratio intensity I_A/I_I value indicates that the ESPT rate of the GFP double mutant T203V/S205A is slow in comparison to other decay processes of the excited ROH form of the chromophore. If the emission life time τ_F for each the ROH (A band) and RO⁻ (I band) is similar, then the ESPT rate constant k_{PT} can be estimated from the two emission bands intensity ratio I^{RO^-}/I^{ROH}

$$k_{PT} = \frac{I^{RO^-}}{I^{ROH}} \cdot \frac{1}{\tau_F} \quad (3)$$

Where τ_F is the radiative lifetime of the ROH and the RO⁻ forms assuming that they are similar. One can see that the ESPT rate constant k_{PT} increases with an increase of the ratio I^{RO^-}/I^{ROH} . In the case for the GFP double mutant T203V/S205A the ROH (A band) and RO⁻ (I band) intensities are similar and thus equation (3) is not accurate in determining the k_{PT} value. In the current study we use a more accurate analysis to estimate the ESPT rate constant k_{PT} using both the time-resolved emission results and the steady-state measurements. We apply a series of basic equations of fluorescence quantum

efficiency and PT efficiency with the rate constants depleting the population of the excited states that lead to bands A and I emissions.

The fluorescence quantum efficiency of the protonated form ROH that indicates the A band emission is given by

$$\Phi^{ROH} = \frac{k_r}{k} \quad (4)$$

$$k = k_r + k_{nr} + k_{PT} \quad (5)$$

where k_r is a radiative rate constant, k_{nr} is the non-radiative rate constant and k_{PT} is the ESPT rate constant. The value of k is obtained from the time-resolved emission analysis.

The fluorescence quantum efficiency of the deprotonated form RO⁻ that indicates the I band emission is given by

$$\Phi^{RO^-} = \frac{k'_r}{k'_r + k'_{nr}} \quad (6)$$

where k'_r is a radiative rate constant and k'_{nr} is a non-radiative rate constant.

The ESPT quantum efficiency is given by

$$\Phi^{PT} = \frac{k_{PT}}{k} \quad (7)$$

The fluorescence quantum efficiency of RO^{-*}, when the chromophore is excited from the ground state protonated ROH form and undergoes an ESPT process is given by

$$\Phi_{exROH}^{RO^-} = \Phi_{PT} \times \Phi^{RO^-} \quad (8)$$

The fluorescence quantum efficiency of the RO⁻ of GFP is usually very high³⁷ $\Phi^{RO^-} \geq 0.85$, therefore for simplicity we assume that is $\Phi^{RO^-} = 1$, and thus equation 5 is simplified:

$$\Phi_{exROH}^{RO^-} = \Phi_{PT} \quad (9)$$

The ratio of the fluorescence quantum yield $\Phi_{exROH}^{RO^-} / \Phi^{RO^-}$ is given by

$$\frac{\Phi_{exROH}^{RO^-}}{\Phi^{RO^-}} = \frac{k_{PT}}{k_r} \quad (10)$$

The measured fluorescence intensity of a sample is proportional to the fluorescence quantum yields (equation (10)) and to the sample ROH and RO⁻ chromophore's absorption:

$$\frac{I_{exROH}^{RO^-}}{I^{RO^-}} = \frac{k_{PT}}{k_r} \cdot \frac{A_{ROH}}{A_{RO^-}} \quad (11)$$

where $I_{exROH}^{RO^-}$ and I^{RO^-} are the RO⁻ fluorescence emission band intensities obtained from the steady-state emission of the GFP double mutant T203V/S205A samples when excited at 400nm and 475nm, respectively. The absorbance ratio A_{ROH}/A_{RO^-} is obtained from the absorption spectrum of the GFP double mutant T203V/S205A. The chromophore's radiative rate constant k_r is $\sim 3 \times 10^8 \text{ sec}^{-1}$.

We find that for the T203V/S205A mutant $\Phi_{exROH}^{RO^-} / \Phi^{RO^-} \cong 20$ and that the $A_{ROH} / A_{RO^-} \cong 20$ and thus $k_{PT} \sim k_r$ where $k_r = 3 \times 10^8 \text{ s}^{-1}$. We therefore conclude that k_{PT} is about $3 \times 10^8 \text{ s}^{-1}$. This value is ~ 350 times smaller than the value of wt-GFP $k_{PT} \sim 1.2 \times 10^{11} \text{ s}^{-1}$. The non-radiative rate constant of the RO⁻ is larger than the radiative rate and is given by $k_{nr} = k - k_r - k_{PT}$ and its calculated value is $\sim 6 \times 10^8 \text{ s}^{-1}$ twice that of k_{PT} and k_r .

The values of $k_{PT}^{D_2O}$ and $\Phi_{PT}^{D_2O}$ are not so simple to derive and the error in the derived values are large $\pm 25\%$. In H₂O the ESPT rate constant of the S203V/S205A mutant is of the same value as the radiative rate and the nonradiative rate is twice larger; $k_{PT} \approx k_r = 3.3 \times 10^8 \text{ s}^{-1}$ and $k_{nr} \approx 6 \times 10^8$.

In D₂O we find KIE=2.75 for k_{PT} , i.e. $k_{PT}^{D_2O} = 1.2 \times 10^8$. We assume that k_r and $k_{nr}^{D_2O}$ are the same as in H₂O. This could also be written as $k_{nr}^{D_2O} = 5.5 k_{PT}^{D_2O}$. It means that the fluorescence decay rate constant $k^{D_2O} = k_r + k_{nr} + k_{PT}^{D_2O}$ is only weakly influenced by $k_{PT}^{D_2O}$ and the main parameters that determine k , the fluorescence decay rate, are k_r and k_{nr} . The calculated proton transfer quantum yield is rather low $\Phi_{PT}^{D_2O} = k_{PT}^{D_2O} / k^{D_2O} \cong 0.1$ and therefore the intensity of the RO⁻ band of the steady-state spectrum shown in Figure 3 is small.

The proton transfer mechanism in the GFP double mutant T203V/S205A

The most interesting question we aimed to tackle in this study is: why does the PT process does not occur for the GFP double mutant T203V/S205V, while for the GFP double mutant T203V/S205A it does occur. We would expect that in both double mutants the PT process will not occur, because the proton wire mechanism is blocked, as seen in schemes 1 and 2 and Figure 1. The only difference between the two mutants is the mutation of the Ser205 by a Valine residue or an Alanine residue, in which both are hydrophobic, though Valine has a larger aliphatic group than Alanine. To address this question we applied MD simulations to both mutants and followed the difference between the structures of these mutants along the MD simulations.

We followed the locations of water molecules in the environment of the chromophore in both mutants in aim to examine possible alternative proton-wire pathways. We found that the Glu222 is surrounded by water molecules that form hydrogen bond interactions with the Glu222 (Figure 9a). We examined the averaged number of the water molecules around the Glu222 along the MD simulations (Figure S4). One can see that only one water molecule appears around the Glu222 along the MD simulations and most of the time of the simulations the water molecules do not appear near the Glu222, thus this water molecule had not been found in the x-ray crystallography. We note that mutation in Glu222 will not affect the spectral potential of T203V/S205V, while in the wt-GFP it affects. In any case, these water molecules are relatively far from the phenol group of the chromophore, but nearby the imidazole group of the chromophore. Yet, the carbonyl oxygen atoms of the Glu222 that are near the imidazole group can be protonated only by the phenol proton, therefore this optional proton wire transfer is impossible. We also noticed that one or two water molecules are near the phenol group of the chromophore and the backbone O atom of the Asn146 (Figure 9b). However, since the pK_a of Asn146 is relatively high (around 16-17) it is unlikely that the Asn146 will be an acceptor for a proton, therefore this optional mechanism is ruled out.

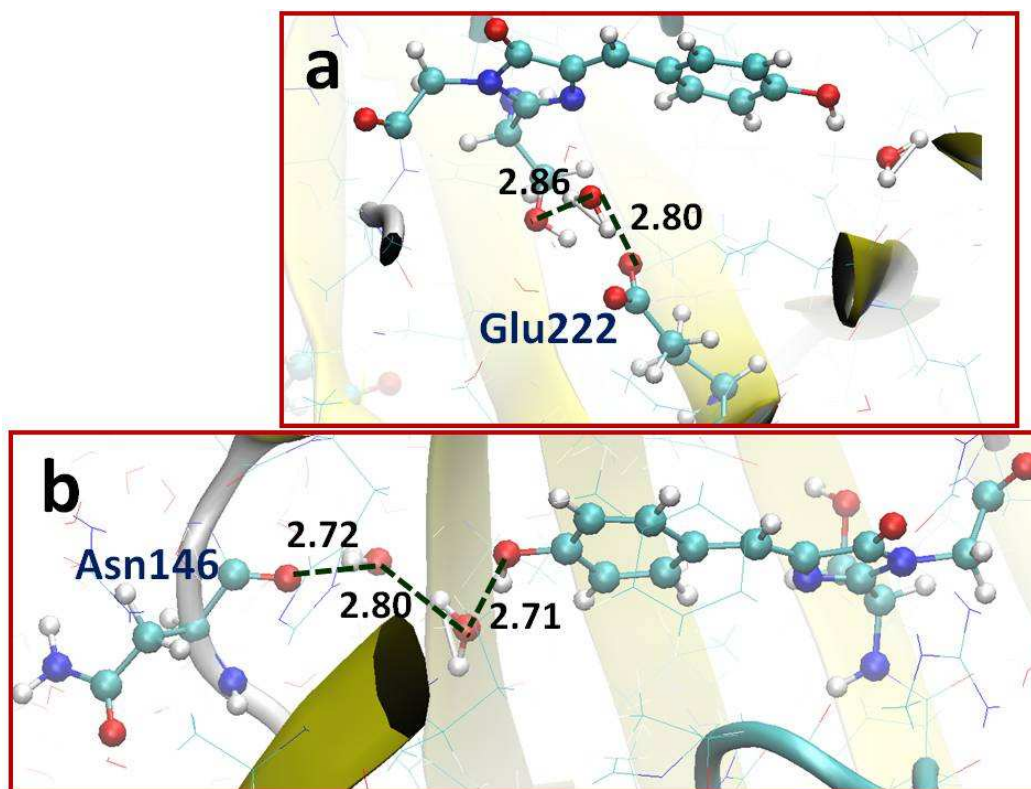


Figure 9: Snapshots from MD simulations of optional proton wire pathways that impossible in the GFP double mutant T203V/S205A. (a) O atom of the imidazole group - H₂O - Glu222. (b) O atom of the phenol group - H₂O - Asn146.

Finally, the crystal structure of the GFP double mutant T203V/S205A (as well as WT-GFP and GFP T203V) exhibits one water molecule, adjacent to the chromophore, that forms a hydrogen bond with the phenol group of the chromophore. Therefore, we searched around this environmental domain and found out that other water molecules from the bulk can occasionally form a chain of hydrogen bond interactions with this water molecule next to the chromophore's phenol OH. This interesting finding led us to propose that the PT in these double mutants may be from the phenol group to the nearby water molecule and subsequently the proton is transferred to the other water molecules that enter the barrel from the bulk (Figure 10). Interestingly, one can see from the simulations that the water molecules from the bulk enter the β -barrel via a “hole”

between the two β -strands. The “hole” domain is nearby the chromophore and consists of residues Glu142-Asn146 in one β -strand and residues Arg168-Glu172 in the second β -strand. Figure S5 illustrates the averaged number of water molecules along the MD simulations for the residues that along the two β -strands that are pointed to the “hole” where the water molecules insert from the bulk. One can see that the residues of one of the β -strand Glu142, Asn144 and Asn146 are solvated (1-3 water molecules). The residues in the second β -strand that are solvated are Arg168 and Glu172 (1-3 water molecules). Interestingly, the solvated residues in the “hole” domain are all charged. We further measured the $C\alpha$ backbone-backbone distance between two opposite residues in the two β -strands (Figure S6). One can see that these distances are above 6 Å and thus allow to water molecules to insert from the bulk to the interior domain of the GFP, nearby the chromophore. Finally, we computed the RMSD of residues 140-148 in one β -strand and residues 166-174 in the second β -strands (Figure S7). The RMSD results demonstrate that these residues contribute to the opening of the two β -stands. Finally, we assume that mutations in these two β -stand fragments may affect the slow mechanism of proton transfer.

It may even prevent the phenomenon of proton transfer. We suggest that this PT process of the “chain-water molecules” is not a frequent phenomenon, because the appearance of this “chain-water molecules” is only in a small number of snapshots along the MD simulations. This may explain the relatively slow PT that had been observed from the steady-state spectrum and the time-resolved emission decay spectrum.

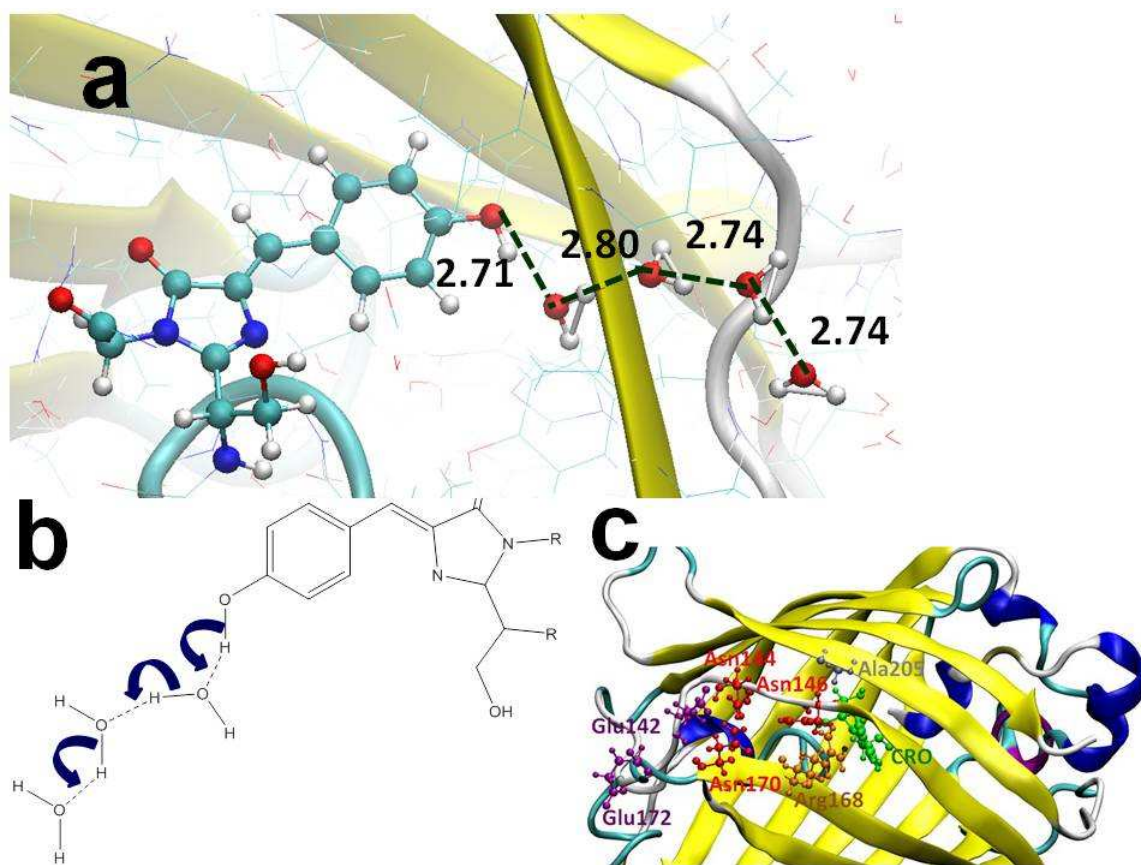


Figure 10: A proposed proton wire mechanism for the GFP double mutant T203V/S205A: proton transfer from the phenol group of the chromophore to the water in the bulk, via a “hole” between two β -strands of the β -barrel of the GFP. (a) A snapshot from MD simulations. (b) A schematic illustration of the proposed mechanism.

Unfortunately, in crystal structure of GFP T203V/S205A obtained at 100 K, this region of the polypeptide chain forms the major intermolecular contact between the two monomers in the asymmetric unit, with Asn146 close to center of the interaction region. Therefore, in the crystal structure the conformations and mobilities of individual residues within this region may not be representative of the conformations and mobilities accessible to the molecule at room temperature, in solution.

It should be noted that this PT mechanism had been found in the simulations for both the GFP double mutants T203V/S205A and T203V/S205V. Therefore, we examined the

fraction of the “chain-water molecules” events along the simulations of 60ns for both mutants (Figure 11). We followed the number of snapshots that illustrate the chromophore-water-water proton wire along the MD simulations (Figure 11a) and the number of the snapshots that demonstrate a water molecule that appears near the water molecule that is nearby to the chromophore (Figure 11b). It should be noted that when these two water molecules appear in the chromophore-water-water proton wire, we noticed on other water molecules in the bulk that form hydrogen bond interactions. Therefore, we focused only on the distance between the water molecule which is near the chromophore and the water molecule that is near this water molecule.

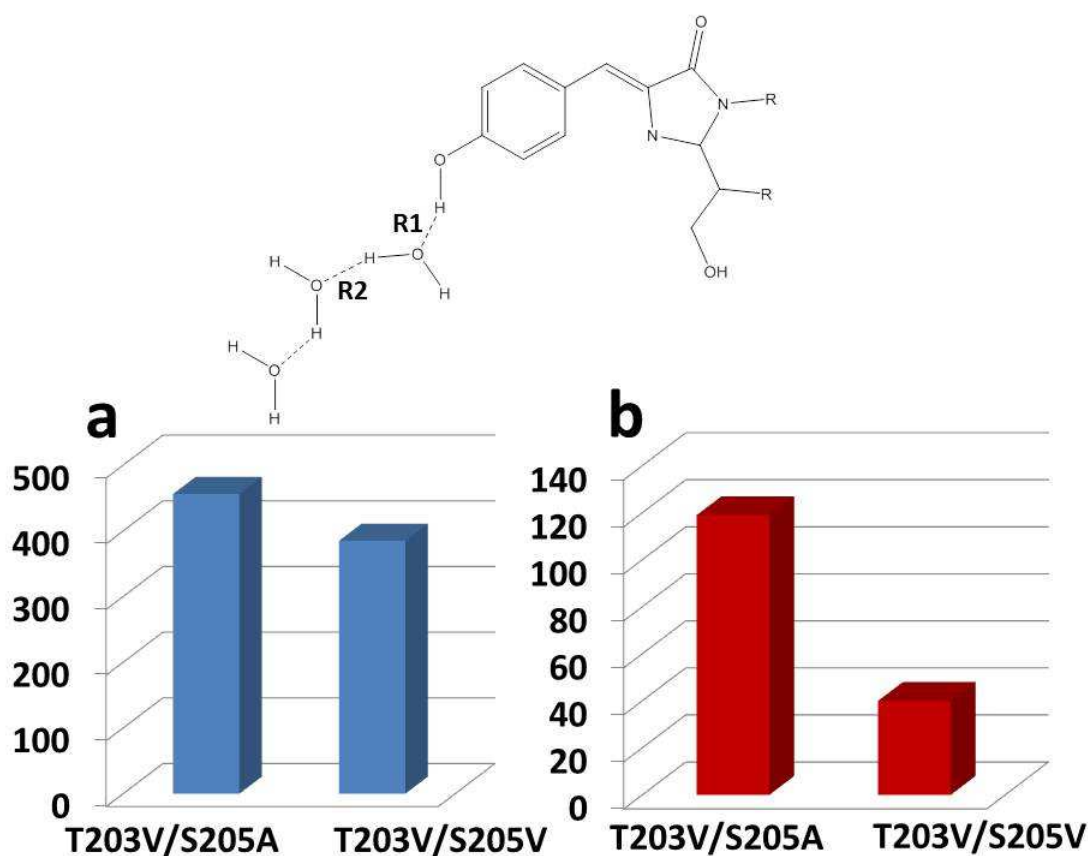


Figure 11: The number of the proton-wire events along the MD simulations in the GFP double mutants T203V/S205A and T203V/S205V: (a) The number of the snapshots that demonstrate distances of $R1 \leq 2.86 \text{ \AA}$ and $R2 \leq 3.1 \text{ \AA}$. (b) The number of residence times of water molecules flowing from the bulk solvent into the active site that demonstrates cutoff distances of $R2 \leq 3.1 \text{ \AA}$.

One can see that the number of the snapshots that illustrate “chromophore-water-water” proton wire in the GFP double mutant T203V/S205A is larger by more than ~20% than that of the GFP double mutant T203V/S205V. Moreover, the number of the water molecules which are near the water molecule next to the chromophore of the double mutant T203V/S205A is 3 times larger than that of the double mutant T203V/S205V. The number of residence times of water molecules flowing from the bulk solvent into the active site that demonstrates cutoff distances of R2 is larger by more 70% than in T203V/S205V, as seen in Figure 11b. This event is necessary for “chromophore-water-water” proton wire. This finding may explain the occurrence of the PT in the GFP double mutant T203V/S205A and the lack of the ESPT in GFP double mutant T203V/S205V. When the excited-state proton transfer rate constant k_{PT} is smaller than the radiative rate k_r of the ROH form than the ESPT efficiency decreases and for $k_{PT} \ll k_r$ the efficiency is too low for detection. The ESPT efficiency is given by eq. 5. The smaller number of events of chromophore-water-water for T203V/S205A reduces the value of k_{PT} and hence decreases Φ_{PT} below the detection level. The small fraction of events of water molecules nearby the water that is near to the chromophore in the GFP double mutant T203V/S205V (~40 events, which is 0.67%) demonstrates impossible PT process. However, the relatively large fraction of events in the GFP double mutant T203V/S205A (~120 events, which is 2%) compared to the GFP double mutant T203V/S205V shows that that the PT is possible for this mutant. Yet, we propose that this PT process is slow relatively to the wt-GFP, because the small fraction of the events of performance of other water molecules. Finally, we note that in the crystal structures of both mutants only one water molecule had been observed - the water molecule which is near the chromophore hydroxyl. Our simulations for example for the GFP double mutant T203V/S205A show that the water molecule which is near the chromophore hydroxyl is replaced by another water molecule (Figure S8). Therefore, the phenol group of the chromophore has only a water molecule around along all of the 60 ns of the simulations. These water molecules are long-lived waters and thus can be found in the x-ray crystallography. The transient water molecules proposed here to participate in ESPT are not expected to be observable in the *static* crystallographic structures for two reasons. First, the diffraction data were collected on crystals flash frozen at 100 K and second, the lifetimes of events associated

with the presence of water molecules originating from the bulk are expected to be short, and thus do not contribute to long term average changes in the protein structure.

We further examined the averaged number of water molecules near the two β -strands in the “hole” domain in the wt-GFP and the GFP double mutant T203V/S205V (Figures S9 and S10). Interestingly, similarly to the two double mutant variant that are examined in this study, some of the residues along these two β -strands in the wt-GFP are also solvated and thus we suggest that the “chromophore-water-water” proton wire also appears in wt-GFP, however, since the PT is relatively fast compare to the other single and double mutants of GFP, this proton-wire is a minor mechanism in the wt-GFP. For the GFP double mutant T203V/S205V the probability for the occurrence of this proton-wire mechanism is low as seen in Figure 11.

Conclusions

The GFP is prototypical example of a biological system in which PT play a role in the mechanism of activity. The chromophore in the wt-GFP is a ‘photoacid-like’ species and thus it has the ability to transfer a proton to the nearby ‘base-like’ species the Glu222, via a proton wire, as seen in scheme 1. Mutations of S205V or S205A in the GFP led to a relatively slow PT compared to the wt-GFP: for the S205V GFP mutant it is 30 time slower than the wt-GFP and for the S205A it is 15 times slower than the wt-GFP. Furthermore, these mutations led to an alternative proton wire (scheme 2), in which the residue T203 play a key role in the PT. Therefore, we expect that double mutations of residues T203 and S205 may block the PT process in the GFP. Previously, we showed that indeed the GFP double mutant T203V/S205V does not present PT, since these two mutants block the proton-wire pathway. Furthermore, the GFP double mutant T203V/S205V showed an emission which originates from the A band in the blue spectral region.¹⁸

In this study, we investigated the GFP double mutant T203V/S205A and surprisingly both the time-resolved emission spectroscopy and the steady-state emission spectra results suggested that a slow PT occurs with relatively small quantum efficiency: First, the PT rate in this mutant is ~ 350 times slower than that of the wt-GFP. Second, the KIE (I_{RO^-}/I_{ROH}) is 2.75, which is relatively large and therefore supports PT in the double

mutant. Previously, we have shown that the KIE of the wt-GFP and other single mutants such as S205V is ~ 5 . Third, the non-radiative rate of the excited state of the protonated form of the chromophore is twice faster than the PT rate, and thus the quantum efficiency is small (0.25 for H₂O and 0.1 for D₂O).

To understand why in the GFP double mutant T203V/S205V the PT process is not observed, while in the GFP double mutant T203V/S205A a slow PT occurs with relatively low efficiency, we ran all-atom explicit MD simulations for both T203V/S205V and T203V/S205A mutants. We examined all alternative proton-wire pathways and concluded that only one possible proton-wire pathway could explain the PT process in the GFP double mutant T203V/S205A. We therefore suggest a novel alternative proton-wire in which the proton transfers from the O atom of the phenol group of the chromophore to a permanent nearby water molecule and then to water molecules that transiently penetrate the structure from the bulk. The phenomenon of a proton-wire consisting of two water molecules from a photoacid to bulk water had been suggested by Pérez-Lustres et al³⁸ in acetonitrile/water mixtures. We found that MD simulations also predict the appearance of a transient proton-wire pathway in the GFP double mutant T203V/S205V. However, in the T203V/S205V mutant the transient pathway appears with a relatively smaller fraction of proton-wire events than in T203V/S205A, which may explain why PT is not observed in the former. The smaller size of the alanine versus valine side chain at position 205 is consistent with the suggestion from MD simulations that the chromophore cavity in T203V/S205A is less well packed than in T203V/S205V, and hence more accessible to solvent molecules entering from the bulk.

This study enhances future work on many other mutants that can be performed near the chromophore of the wt-GFP. Future work will need to focus on the study of whether a PT occurs in various mutants and if so, to investigate alternative proton-wire mechanisms that occur in these mutants.

Acknowledgment

This project is funded by the FP7-PEOPLE-2011-CIG (YM; CIG 303741). DH and SJR were funded by the BSF. SJR acknowledges support from the National Science

Foundation, grant MCB-1021374. All simulations were performed using the high-performance computational facilities of the Miller lab in the BGU HPC computational center. The support of the BGU HPC computational center staff is greatly appreciated.

References

- (1) Prasher, D. C.; Eckenrode, V. K.; Ward, W. W.; Prendergast, F. G.; Cormier, M. J.: Primary structure of the *Aequorea victoria* green-fluorescent protein. *Gene* **1992**, *111*, 229-33.
- (2) Siererol-Piquer, M. S.; Cebrian-Silla, A.; Alfaro-Cervello, C.; Gomez-Pinedo, U.; Soriano-Navarro, M.; Verdugo, J. M.: GFP immunogold staining, from light to electron microscopy, in mammalian cells. *Micron* **2012**, *43*, 589-99.
- (3) Zimmer, M.: Green fluorescent protein (GFP): applications, structure, and related photophysical behavior. *Chemical reviews* **2002**, *102*, 759-81.
- (4) Tsien, R. Y.: The green fluorescent protein. *Annual review of biochemistry* **1998**, *67*, 509-44.
- (5) Morise, H.; Shimomura, O.; Johnson, F. H.; Winant, J.: Intermolecular energy transfer in the bioluminescent system of *Aequorea*. *Biochemistry* **1974**, *13*, 2656-62.
- (6) Remington, S. J.: Fluorescent proteins: maturation, photochemistry and photophysics. *Current opinion in structural biology* **2006**, *16*, 714-21.
- (7) Meech, S. R.: Excited state reactions in fluorescent proteins. *Chemical Society reviews* **2009**, *38*, 2922-34.
- (8) Cubitt, A. B.; Heim, R.; Adams, S. R.; Boyd, A. E.; Gross, L. A.; Tsien, R. Y.: Understanding, improving and using green fluorescent proteins. *Trends in biochemical sciences* **1995**, *20*, 448-55.
- (9) Chattoraj, M.; King, B. A.; Bublitz, G. U.; Boxer, S. G.: Ultra-fast excited state dynamics in green fluorescent protein: multiple states and proton transfer. *Proceedings of the National Academy of Sciences of the United States of America* **1996**, *93*, 8362-7.
- (10) Herman, B.: *Resonance energy transfer microscopy. In Fluorescence Microscopy of Living Cells in Culture.*; Academic Press, San Diego, CA. , 1989.
- (11) Rizzuto, R.; Brini, M.; De Giorgi, F.; Rossi, R.; Heim, R.; Tsien, R. Y.; Pozzan, T.: Double labelling of subcellular structures with organelle-targeted GFP mutants in vivo. *Current biology : CB* **1996**, *6*, 183-8.
- (12) Mitra, R. D.; Silva, C. M.; Youvan, D. C.: Fluorescence resonance energy transfer between blue-emitting and red-shifted excitation derivatives of the green fluorescent protein. *Gene* **1996**, *173*, 13-7.
- (13) Ormo, M.; Cubitt, A. B.; Kallio, K.; Gross, L. A.; Tsien, R. Y.; Remington, S. J.: Crystal structure of the *Aequorea victoria* green fluorescent protein. *Science* **1996**, *273*, 1392-5.
- (14) Stoner-Ma, D.; Jaye, A. A.; Ronayne, K. L.; Nappa, J.; Tonge, P. J.; Meech, S. R.: Ultrafast Electronic and Vibrational Dynamics of Stabilized A State Mutants of the Green Fluorescent Protein (GFP): Snipping the Proton Wire. *Chemical physics* **2008**, *350*, 193-200.
- (15) Jung, G.; Wiehler, J.; Zumbusch, A.: The photophysics of green fluorescent protein: influence of the key amino acids at positions 65, 203, and 222. *Biophysical journal* **2005**, *88*, 1932-47.

- (16) van Thor, J. J.; Zanetti, G.; Ronayne, K. L.; Towrie, M.: Structural events in the photocycle of green fluorescent protein. *The journal of physical chemistry. B* **2005**, *109*, 16099-108.
- (17) Stoner-Ma, D.; Jaye, A. A.; Matousek, P.; Towrie, M.; Meech, S. R.; Tonge, P. J.: Observation of excited-state proton transfer in green fluorescent protein using ultrafast vibrational spectroscopy. *Journal of the American Chemical Society* **2005**, *127*, 2864-5.
- (18) Shu, X.; Leiderman, P.; Gepshtein, R.; Smith, N. R.; Kallio, K.; Huppert, D.; Remington, S. J.: An alternative excited-state proton transfer pathway in green fluorescent protein variant S205V. *Protein science : a publication of the Protein Society* **2007**, *16*, 2703-10.
- (19) Simkovitch, R.; Huppert, A.; Huppert, D.; Remington, S. J.; Miller, Y.: Proton Transfer in Wild-Type GFP and S205V Mutant Is Reduced by Conformational Changes of Residues in the Proton Wire. *The journal of physical chemistry. B* **2013**, *117*, 11921-31.
- (20) Kissinger, C. R.; Gehlhaar, D. K.; Fogel, D. B.: Rapid automated molecular replacement by evolutionary search. *Acta crystallographica. Section D, Biological crystallography* **1999**, *55*, 484-91.
- (21) *The CCP4 suite: programs for protein crystallography. Acta Crystallogr. sect. D. 50: 760-763*, 1994.
- (22) Murshudov, G. N.; Skubak, P.; Lebedev, A. A.; Pannu, N. S.; Steiner, R. A.; Nicholls, R. A.; Winn, M. D.; Long, F.; Vagin, A. A.: REFMAC5 for the refinement of macromolecular crystal structures. *Acta Crystallographica Section D* **2011**, *67*, 355-367.
- (23) Murshudov, G. N.; Vagin, A. A.; Dodson, E. J.: Refinement of Macromolecular Structures by the Maximum-Likelihood Method. *Acta Crystallographica Section D* **1997**, *53*, 240-255.
- (24) Emsley, P.; Cowtan, K.: Coot: model-building tools for molecular graphics. *Acta crystallographica. Section D, Biological crystallography* **2004**, *60*, 2126-32.
- (25) Kalé, L.; Skeel, R.; Bhandarkar, M.; Brunner, R.; Gursoy, A.; Krawetz, N.; Phillips, J.; Shinozaki, A.; Varadarajan, K.; Schulten, K.: NAMD2 : Greater Scalability for Parallel Molecular Dynamics. *Journal of Computational Physics* **1999**, *151*, 283.
- (26) MacKerell, A. D.; Bashford, D.; Bellott, M.; Dunbrack, R. L.; Evanseck, J. D.; Field, M. J.; Fischer, S.; Gao, J.; Guo, H.; Ha, S.; Joseph-McCarthy, D.; Kuchnir, L.; Kuczera, K.; Lau, F. T. K.; Mattos, C.; Michnick, S.; Ngo, T.; Nguyen, D. T.; Prodhom, B.; Reiher, W. E.; Roux, B.; Schlenkrich, M.; Smith, J. C.; Stote, R.; Straub, J.; Watanabe, M.; Wiorkiewicz-Kuczera, J.; Yin, D.; Karplus, M.: All-atom empirical potential for molecular modeling and dynamics studies of proteins. *Journal of Physical Chemistry B* **1998**, *102*, 3586-3616.
- (27) Vendrell, O.; Gelabert, R.; Moreno, M.; Lluch, J. M.: Potential energy landscape of the photoinduced multiple proton-transfer process in the green fluorescent protein: classical molecular dynamics and multiconfigurational electronic structure calculations. *Journal of the American Chemical Society* **2006**, *128*, 3564-74.

- (28) Mahoney, M. W.; Jorgensen, W. L.: A five-site model for liquid water and the reproduction of the density anomaly by rigid, nonpolarizable potential functions. *J Chem Phys* **2000**, *112*, 8910-8922.
- (29) Jorgensen, W. L.; Chandrasekhar, J.; Madura, J. D.; Impey, R. W.; Klein, M. L.: Comparison of simple potential functions for simulating liquid water. *The Journal of Chemical Physics* **1983**, *79*, 926-935.
- (30) Feller, S. E.; Zhang, Y. H.; Pastor, R. W.; Brooks, B. R.: Constant-Pressure Molecular-Dynamics Simulation - the Langevin Piston Method. *J Chem Phys* **1995**, *103*, 4613-4621.
- (31) Martyna, G. J.; Tobias, D. J.; Klein, M. L.: Constant-Pressure Molecular-Dynamics Algorithms. *J Chem Phys* **1994**, *101*, 4177-4189.
- (32) Darden, T.; York, D.; Pedersen, L.: Particle mesh Ewald: An N [center dot] log(N) method for Ewald sums in large systems. *The Journal of Chemical Physics* **1993**, *98*, 10089-10092.
- (33) Essmann, U.; Perera, L.; Berkowitz, M. L.; Darden, T.; Lee, H.; Pedersen, L. G.: A smooth particle mesh Ewald method. *The Journal of Chemical Physics* **1995**, *103*, 8577-8593.
- (34) Connolly, M. L.: The molecular surface package. *Journal of molecular graphics* **1993**, *11*, 139-41.
- (35) Huang, K.: *Physics*; A. proc. R. Soc. London, 1950.
- (36) Fraser, R. D. B., Suzuki, E.: *Spectral Analysis*; Balckburn, J.A. Ed. (Marcel Dekker, New York), 1970.
- (37) Zimmer, M.: Green Fluorescent Protein (GFP) : Applications , Structure , and Related Photophysical Behavior. *Chemical Reviews* **2002**, *102*, 759.
- (38) Perez-Lustres, J. L.; Rodriguez-Prieto, F.; Mosquera, M.; Senyushkina, T. A.; Ernsting, N. P.; Kovalenko, S. A.: Ultrafast proton transfer to solvent: molecularity and intermediates from solvation- and diffusion-controlled regimes. *Journal of the American Chemical Society* **2007**, *129*, 5408-18.